

# Center-to-limb variation of the enigmatic Na I D<sub>1</sub> and D<sub>2</sub> polarization profiles

J.O. Stenflo<sup>1</sup>, A. Gandorfer<sup>1</sup>, and C.U. Keller<sup>2</sup>

<sup>1</sup> Institute of Astronomy, ETH Zentrum, 8092 Zurich, Switzerland

<sup>2</sup> National Solar Observatory, P.O. Box 26732, Tucson, AZ 85726-6732, USA

Received 8 December 1999 / Accepted 17 January 2000

**Abstract.** The remarkable polarization structure of the Na I D<sub>1</sub> and D<sub>2</sub> lines that is due to coherent scattering has remained an enigma, since it has not yet been possible to find an explanation that is consistent with both current understanding of quantum mechanics and the astrophysical properties of the Sun's atmosphere. To guide future theoretical efforts we have here explored the detailed center-to-limb variation of the linearly polarized profiles in non-magnetic regions. In particular we find that the unexplained narrow polarization peaks in the Doppler cores of the two lines become even more pronounced with respect to the relative profile shape as we move away from the limb towards the center of the solar disk.

**Key words:** polarization – scattering – Sun: magnetic fields – atomic processes – techniques: polarimetric

## 1. Introduction

One of the most enigmatic features of the “second solar spectrum” (the linearly polarized spectrum that is due to coherent scattering processes on the Sun) has been the spectral structure across the Na I D<sub>1</sub> 5895.94 and D<sub>2</sub> 5889.97 Å lines. Although the general shape of the polarized profile with its remarkable signature of quantum-mechanical interference between the two scattering transitions was uncovered already in 1978 in observations at the National Solar Observatory (NSO), both at NSO/Sac Peak and NSO/Kitt Peak (Stenflo et al. 1980, 1983), it was only with the much higher sensitivity of the ZIMPOL system (Zurich **I**maging **P**olarimeter, cf. Povel 1995) that the polarization peaks in the Doppler cores of the two lines could be recorded with convincing precision (Stenflo & Keller 1996, 1997). The core peak in the D<sub>1</sub> line has been the main mystery, since according to standard quantum mechanics such a line that represents a  $J = \frac{1}{2} \rightarrow \frac{1}{2} \rightarrow \frac{1}{2}$  scattering transition should be intrinsically unpolarizable.

An elegant explanation of the core peaks was recently proposed by Landi Degl'Innocenti (1998, 1999) in terms of a combination of hyperfine structure splitting and optical pumping. Due to the nuclear spin of  $\frac{3}{2}$  for sodium the  $J = \frac{1}{2}$  lower and

upper states get split into hyperfine states with different quantum numbers, which are polarizable in principle. To obtain a net polarization for the emitted radiation it is however necessary that the initial, lower state of the scattering transition is polarized (aligned). This may be achieved by an optical pumping process. While alignment in the excited state is induced by the anisotropic excitation, the spontaneous emission process transfers some of that alignment to the lower state. With many such transitions a statistical equilibrium becomes established that leaves the lower level in a polarized state. This ground-state polarization can be imprinted on the polarization of the scattered light, making the D<sub>1</sub> line emission polarized. With this theoretical framework Landi Degl'Innocenti (1999) could model the polarized line profiles for different center-to-limb distances.

This explanation however requires that the alignment of the lower state survives destruction by magnetic fields (Hanle depolarization) and collisions during its life time, until the next radiative excitation. Since the life time of the lower state is longer by approximately two orders of magnitudes as compared with the excited state, it is correspondingly more vulnerable to such destruction. Landi Degl'Innocenti (1998) therefore concluded that either the field strength (of a small-scale field with random orientations of the field vectors) would need to be smaller than about 10 mG, or the field orientation would have to be very close to vertical, to make the Hanle depolarization effects sufficiently small. However, Zeeman-effect observations have shown that the magnetic field in the lower chromosphere (where the cores of the Na I D<sub>1</sub> and D<sub>2</sub> lines are formed) is highly inclined with a canopy-like structure (Giovanelli 1980; Jones & Giovanelli 1983). Hanle effect observations (Bianda et al. 1998a,b, 1999) also rule out that the magnetic field is everywhere vertical, and show that fields as weak as 10 mG do not exist (at least not with sufficient filling factor), but that the solar atmosphere is instead permeated by fields with a strength on the order of 10 G, which may be turbulent lower down and canopy-like higher up.

We are therefore stuck in a paradoxical situation. There is not even a consensus on whether its resolution is to be found within atomic physics or within astrophysics, although we are convinced (because of the mentioned Hanle-effect evidence from other spectral lines) that the problem is basically one of atomic or quantum physics. Further theoretical progress and modelling need to be guided by qualitatively new observations that can

better constrain the possible physics involved. The objective of the present paper is to provide such new constraints.

## 2. Observed set of polarized line profiles

### 2.1. Effects from magnetic fields and scattered light

The polarization features of the second solar spectrum are expected to have their largest amplitudes in the absence of magnetic fields, since the modification by magnetic fields, via the Hanle effect, manifests itself primarily as depolarization and rotation of the plane of linear polarization. For a spherically symmetric sun and in the absence of magnetic fields the linear polarization increases steeply in amplitude as we approach the solar limb, and the orientation of the electric vector of the scattered radiation is parallel (and in rare cases perpendicular) to the nearest limb. The orientation of the “nearest solar limb” is always perpendicular to the radius vector that connects the disk center with the point of observation, so we could also say that the electric vector is perpendicular (and in rare cases parallel) to the radius vector. To minimize at the present stage the extra complication of magnetic effects we have carried out all our observations far from active regions, always with the slit oriented perpendicular to the radius vector.

Since the non-magnetic scattering polarization should only vary with center-to-limb distance (for a spherically symmetric sun), we usually average the spectra along the slit direction to enhance the polarimetric accuracy, after first having inspected the 2-D spectral images to make sure that significant magnetic-field effects are absent. When we move away from the limb, however, it gets increasingly difficult to avoid magnetic regions with significant Zeeman effect signals, due to the ubiquitous character of solar magnetic fields. Still it is possible to identify the slit portions that are most affected by the Zeeman effect and exclude these portions when determining the polarized line profiles.

The present analysis is based on observations with ZIMPOL I at the McMath-Pierce facility of the National Solar Observatory (Kitt Peak) on March 11 and 12, 1998. ZIMPOL I records two Stokes parameters, here  $I$  and  $Q$ , simultaneously with great precision ( $10^{-5}$  in the degree of polarization). The spectrograph slit is always placed parallel to the nearest solar limb (perpendicular to the radius vector from disk center), and Stokes  $Q$  is defined as linear polarization with the electric vector oriented parallel to the slit. The McMath-Pierce telescope has large and varying instrumental polarization. Before each spectral recording the linear polarization of the telescope is compensated by a tilting glass plate down to a level of about 0.1 %, which is necessary to avoid effects due to the coupling of detector nonlinearities with instrumental polarization (Keller 1996). The remaining instrumental polarization is dominated by  $I \rightarrow Q$  cross talk since  $I$  is always large, while  $U \rightarrow Q$  cross talk is practically non-existent in quiet regions, since  $U$  is always small there. The  $I \rightarrow Q$  cross talk divides out to become spectrally flat in the fractional polarization  $Q/I$ . It therefore simply masquerades as a zero-line offset of the polarization scale.  $V \rightarrow Q$  cross talk is only significant where  $V$ , produced by the longitudinal Zeeman

effect, is fairly large. Since the longitudinal Zeeman effect generates characteristic and nearly anti-symmetric  $V$  profiles and is spatially very structured (along the slit), one can rather easily identify the slit portions where such signatures are present and remove them from the analysis. In practice, if one avoids placing the slit over a limb facula, such contamination from the longitudinal Zeeman effect only becomes a problem rather far from the limb, for  $\mu$  (the cosine of the heliocentric angle)  $\gtrsim 0.4$ .

To determine the center-to-limb variation of the Na I D<sub>2</sub> and D<sub>1</sub>  $Q/I$  profiles that are due to coherent scattering on the Sun we selected the part of the solar disk that appeared to have the smallest facular activity and visible magnetic flux, so that the obtained polarized spectra would as closely as possible be representative of non-magnetic scattering. Since more or less “hidden” magnetic flux exists everywhere on the Sun, our results may well be affected by such magnetic fields via the Hanle effect. Since however the Hanle effect only operates in the Doppler cores of spectral lines but not in their wings, it is only the core peaks in the D<sub>2</sub> and D<sub>1</sub> lines that would be affected. For randomly oriented and spatially unresolved magnetic fields the Hanle effect should always depolarize the linear polarization, which means that the  $Q/I$  amplitudes that we determine in the line cores should represent *lower* limits to the amplitudes that they would have in the ideal, non-magnetic case.

We did careful recordings with ZIMPOL I of the Na I D<sub>2</sub> and D<sub>1</sub> polarization at 11 different  $\mu$  positions on the disk, from  $\mu = 0.05$  to  $\mu = 0.7$ . In addition we did recordings at the extreme limb ( $\mu = 0$ ) and a few arcsec outside the limb, but these recordings are not reliable because of the influence of wide-angle scattered light when we are outside the limb, so they have been discarded. The origin of these polarized scattered light effects has been identified, explained, and modeled by Keller & Sheeley (1999). Quantitative analysis shows that they become insignificant as soon as one is inside the extreme limb, because of the drastically reduced relative contribution of the wide-angle stray light to the observed intensity.

### 2.2. Zero point of the polarization scale

Fig. 1 shows the set of recorded  $Q/I$  spectra at the 11 used center-to-limb positions as well as a representative Stokes  $I$  spectrum (panel to the upper left), obtained at  $\mu = 0.1$ . Since the relative Stokes  $I$  spectrum varies only slowly with center-to-limb distance, we do not display all the  $I$  spectra here. As the spectral field of view was not sufficiently large to cover both the D<sub>2</sub> and D<sub>1</sub> lines at the same time, each spectral panel contains two partially overlapping recordings. Since the  $Q/I$  zero-line offset due to varying instrumental polarization may be different in the two recordings, we have first shifted the zero point of the D<sub>1</sub> recording such that it fits the overlapping portion of the D<sub>2</sub> recording. The overlapping portions are not averaged but plotted separately on top of each other, but since the relative spectral structures reproduce in minute detail, they differ by less than the width of the solid curves in Fig. 1 and are therefore indistinguishable in the figure. The small, odd-looking spectral feature near 5893 Å is for instance no artifact but real, intrinsically solar,

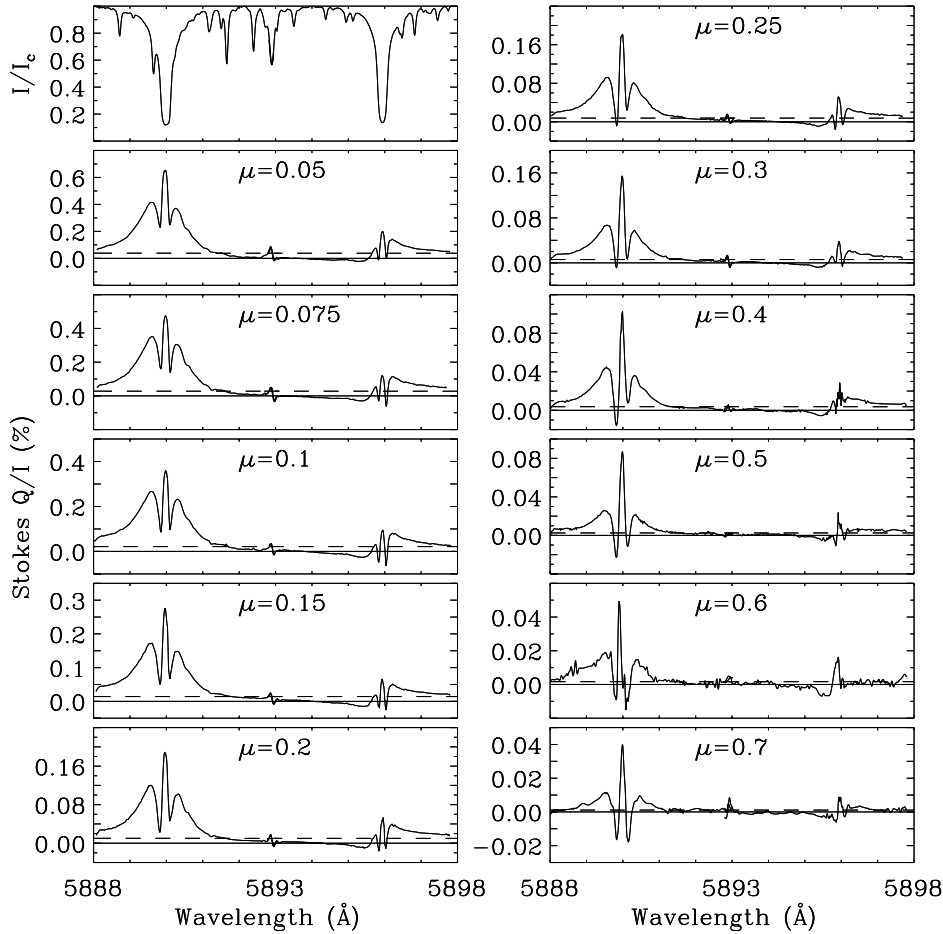


**Fig. 1.** Center-to-limb variation of the profile shapes. The Stokes  $I$  spectrum in the upper left-hand panel has been recorded at  $\mu = 0.1$ . All the other panels display the polarized  $Q/I$  spectra recorded at various  $\mu$ , from 0.05 to 0.7. Note that the scale has been magnified as  $\mu$  increases, to allow a comparison between the relative profile shapes. The horizontal dashed lines represent the level of the continuum polarization

since it reproduces perfectly in the two overlapping recordings and is seen in all other ZIMPOL recordings that we have made of this spectral region. This spectral feature appears to be the combined effect of a depolarizing component, located at the position of an Ni I line, and a polarizing component, located at the position of an Fe I line.

As the next step in the reduction the joint zero point of both recordings has been shifted until the behavior of the  $Q/I$  spectrum at the low and high wavelength portions as well as in the zero-crossing portion between the two lines is consistent with the predicted level of the continuum polarization and with previous observational (Stenflo & Keller 1997) and theoretical (Stenflo 1997) studies. In the April 1995 ZIMPOL I recordings by Stenflo & Keller (1997) for  $\mu = 0.1$  the spectral coverage was much larger than here and included wavelengths sufficiently far from the  $D_2$  and  $D_1$  lines, where the line polarization has asymptotically reached the continuum polarization level. Since no useful empirical determinations of the continuum polarization are available, we use the theoretical continuum polarization values determined from the theory of Fluri & Stenflo (1999) and a model for the average quiet Sun by Fontenla et al. (1993). From our previous work we know how the continuum level is approached in the far line wings at the wavelengths

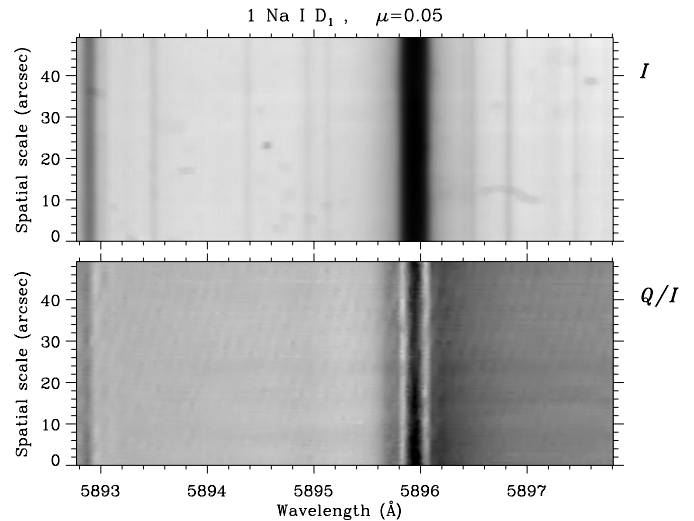


**Fig. 2.** 2-D spectra of Stokes  $I$  and  $Q/I$  for Na I  $D_1$  at  $\mu = 0.05$ . Darker areas mean stronger polarization (in the positive direction), lighter areas weaker or negative polarization. The slit is parallel to the limb. While there is some spatial variation of the polarized core peak maximum, the wing polarization remains spatially invariant. When averaging the  $Q/I$  diagram along the spatial direction, one obtains the 1-D  $Q/I$  profile in the second left panel of Fig. 1

covered by the present recordings. We also know rather well how the Ni I feature near 5893 Å is positioned with respect to the zero-crossing wavelength. This zero crossing is the result of quantum interference between the  $J = \frac{3}{2}$  and  $\frac{1}{2}$  upper states of the D<sub>2</sub> and D<sub>1</sub> transitions and has been studied theoretically rather extensively in the past (Stenflo 1980, 1994, 1997; Landi Degl'Innocenti 1998). Based on all this previous knowledge, it is possible to make a reliable estimate of the true position of the zero point of the polarization scale. This is the way in which the zero points of the various diagrams in Fig. 1 have been determined. The dashed horizontal lines in the diagrams represent the level of the theoretical continuum polarization.

### 2.3. Examples of $Q/I$ profiles

Inspection of the 2-D  $Q/I$  spectra showed that infiltration of the longitudinal Zeeman effect due to  $V \rightarrow Q$  instrumental cross talk was significant only for the recordings with the four largest  $\mu$  values. These recordings could still be used for our analysis after the “contaminated” portions of the slit were excluded or clipped in the data reduction process. For  $\mu = 0.4$  we could use 63 % of the slit, for  $\mu = 0.5$  we used 70 %, for  $\mu = 0.6$  only 25 %, while for  $\mu = 0.7$  we could use 83 %. Due to the small useful slit portion for  $\mu = 0.6$ , the low level of the measured polarization, and remnant magnetic-field effects that could not be cleanly excluded completely, the  $Q/I$  spectrum for  $\mu = 0.6$  is of lesser quality than the others but still good enough to be included here. Conservative wavelet smoothing has been applied to the spectra to suppress noise fluctuations while preserving all spectral structures.

The compressed scale of the plots in Fig. 1, needed to fit all the 11  $Q/I$  spectra into one figure, makes it difficult to appreciate the remarkable profile structure that is really there. To bring out some of this structure more clearly, we plot as an example in Fig. 2 the 2-D  $Q/I$  image for the D<sub>1</sub> recording at  $\mu = 0.05$ . We can here see the main profile features of this line: the large-scale asymmetry between the wing polarizations (light on the left, dark on the right side), and the narrow polarization peak in the line core, surrounded by very narrow and well defined polarization minima.

Another phenomenon that is less pronounced but still visible in Fig. 2 is a spatial variation that is consistent with a Hanle effect interpretation. In a first approximation there are no spatial variations along the 50 arcsec long spectrograph slit. However, if we look carefully, we find that there are spatial variations of the core polarization peak, because the lower spatial portion of the core peak in Fig. 2 is darker than the upper portion, while the wing polarization and the minima surrounding the core do not show any such variation. This is consistent with the expectations from Hanle-effect theory (cf. Omont et al. 1973; Stenflo 1994, 1998), according to which the Hanle effect only operates in the Doppler core of spectral lines but not in their wings (beyond a few Doppler widths). This expectation has been empirically confirmed by Hanle observations in the Sr II 4078 and Ca I 4227 Å lines (Bianda et al. 1998b, 1999). The subtle variation along the slit of the core peak amplitude can therefore be under-

stood in terms of spatially varying Hanle depolarization due to fluctuating magnetic fields. Similar and more pronounced spatially varying Hanle depolarization has previously been noted and displayed for the D<sub>2</sub> line (Stenflo et al. 1998).

Such subtle spatial variations of the core peak polarization are sufficiently small here to be ignored when averaging along the slit to compress the 2-D spectra into the 1-D spectra of Fig. 1. To illustrate the spatially averaged profile shapes in better quantitative detail we show in the upper panel of Fig. 3 the 1-D spectrum that results from compressing the 2-D spectrum of Fig. 2. It is identical to the  $Q/I$  spectrum in the second panel to the upper left of Fig. 1, but we are now able to better appreciate the details of the profile structure. For comparison we show in the lower panel the corresponding profile for  $\mu = 0.10$ .

## 3. Center-to-limb variation of profile parameters

### 3.1. Extracted parameter relations

Inspection of the 11  $Q/I$  diagrams in Fig. 1 immediately reveals several qualitative center-to-limb properties of the profiles. The relative importance of the core polarization peaks *increases* while the surrounding minima decrease and turn negative as we move away from the limb. The ratio between the D<sub>1</sub> and D<sub>2</sub> core amplitudes remains approximately constant, and the width of the D<sub>2</sub> core peak tends to get narrower further from the limb.

To bring out these properties in quantitative detail we have extracted a number of key profile parameters from the  $Q/I$  spectra in Fig. 1 and plotted them vs.  $\mu$  in Fig. 4. The strongest polarization maximum that is not affected by the Hanle effect is the maximum  $p_{D_2 \text{ blue wing}}$  in the blue wing of the D<sub>2</sub> line. Its measured center-to-limb variation is represented by the filled circles in the upper left panel of Fig. 4. While the solid curve is a fit to these data points, the almost indistinguishable dashed curve represents 12 times the theoretical continuum polarization  $p_c$  at the wavelength of the D<sub>2</sub> line, computed from the theory of Fluri & Stenflo (1999) with a model for the average quiet Sun due to Fontenla et al. (1993). The solid curve has been obtained by forming the ratio between the data points and  $p_c$  and then fitting a straight line to these ratio points, since they are found to have a linear dependence on  $\mu$ . The fit then gives us the following expression for the blue wing polarization,

$$p_{D_2 \text{ blue wing}} = (12.3 - 2.0\mu) p_c. \quad (1)$$

This is the formula used to plot the solid curve in the upper left panel.

In the panel to the upper right we have plotted the ratios between the D<sub>2</sub> core polarization amplitude  $p_{D_2 \text{ core max}}$  and  $p_{D_2 \text{ blue wing}}$  (filled circles), as well as the ratios between the average of the two surrounding polarization minima,  $p_{D_2 \text{ core min}}$ , and  $p_{D_2 \text{ blue wing}}$  (open circles). The dashed and dotted curves are second-order polynomial fits to all the points, given by

$$p_{D_2 \text{ core max}}/p_{D_2 \text{ blue wing}} = 1.1 + 3.5\mu - 0.5\mu^2 \quad (2)$$

and

$$p_{D_2 \text{ core min}}/p_{D_2 \text{ blue wing}} = 0.5 - 0.7\mu - 2.8\mu^2. \quad (3)$$

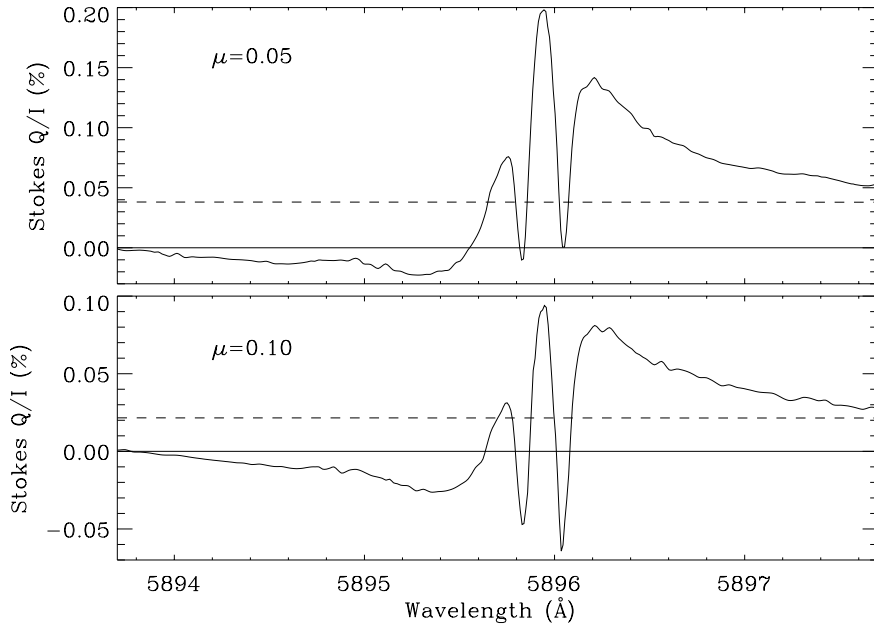


**Fig. 3.** Upper panel: 1-D spectrum of Stokes  $Q/I$  for Na I  $D_1$  at  $\mu = 0.05$ , obtained from the corresponding 2-D spectrum in Fig. 2 by averaging along the slit. It is identical to the  $Q/I$  spectrum in the second left panel of Fig. 1, but it brings out in greater detail the remarkably complex polarization structure of the  $D_1$  line. The horizontal dashed line represents the level of the continuum polarization. Lower panel: The corresponding profile for  $\mu = 0.10$ . It is identical to the  $Q/I$  spectrum in the fourth left panel of Fig. 1

For comparison we have in addition plotted with asterisks the similarly determined normalized average of the polarization minima that surround the core peak in the  $D_1$  line. We have here limited ourselves to the region  $\mu \leq 0.3$ , since only for these  $\mu$  values the structure of the  $D_1$  polarization peak is sufficiently undisturbed by cross-talk effects. In this range we find that  $p_{D_1 \text{ core min}}/p_{D_2 \text{ blue wing}}$  does not vary with limb distance and has an average value of about  $-0.11$ .

In the panel to the lower left we have plotted the ratio between the polarization amplitudes in the cores of the  $D_1$  and the  $D_2$  lines. This ratio is found to be approximately independent of  $\mu$ , with a value of about 0.27. The dashed horizontal line represents the average of the points with  $\mu \leq 0.5$ . The ratio between the polarization maximum in the  $D_1$  red wing and the corresponding maximum in the  $D_2$  blue wing (not plotted here) is about the same ( $\approx 0.3$ ).

Finally the panel to the lower right provides line width information. The filled circles give the total width  $\Delta\lambda$  at half level of the core polarization peak in the  $D_2$  line. The dashed line is a linear fit to the points with  $\mu \leq 0.5$ . It is given by

$$\Delta\lambda_{D_2 \text{ core peak}} = 162 - 45\mu \text{ m}\text{\AA}. \quad (4)$$

The half level used for the width determination is the level that is halfway between  $p_{D_2 \text{ core min}}$  and  $p_{D_2 \text{ core max}}$ . Similarly the asterisks give the corresponding total width for the  $D_1$  line at the half level between  $p_{D_1 \text{ core min}}$  and  $p_{D_1 \text{ core max}}$ , but limited to the region  $\mu \leq 0.3$  to avoid the influence of cross-talk effects. The dotted line is a fit given by

$$\Delta\lambda_{D_1 \text{ core peak}} = 134 - 95\mu \text{ m}\text{\AA}. \quad (5)$$

The  $D_2$  and  $D_1$  polarization peaks are much narrower than the corresponding intensity profiles. For comparison we give as open triangles the total width at half the minimum level of the  $D_1$  intensity profile, which in contrast to the  $D_2$  intensity profile

is not significantly affected by blends. The fit in the form of a dashed-dotted line is given by

$$\Delta\lambda_{D_1 \text{ I profile}} = 306 + 110\mu \text{ m}\text{\AA}. \quad (6)$$

The polarization peaks are thus narrower by a factor of two or more as compared with the intensity profile. This factor increases towards disk center.

### 3.2. Influence of the finite spectral resolution

Since the core polarization peaks in the  $D_1$  and  $D_2$  lines are so narrow, they can only be revealed in observations with sufficient spectral resolution. In our observations the dominating factor that determines the spectral resolution is the geometrical width of the entrance slit, which when optically mapped onto the spectral focus is close to  $40 \text{ m}\text{\AA}$ . The effective smearing width is expected to be somewhat larger than this, since there are other factors (including pixel width and data reduction procedures) that also contribute to the spectral resolution.

To get a better feeling for the amount of spectral smearing in our data we have determined the total width at half the minimum level of a telluric water ( $\text{H}_2\text{O}$ ) line at  $5891.660 \text{ \AA}$  and plotted the results as the crosses and the horizontal solid line in the lower right panel of Fig. 4. The half width is found to be  $85 \text{ m}\text{\AA}$ , independent of  $\mu$ . We have then similarly determined the half width from an FTS spectrum at disk center. The FTS spectrum, which may be regarded as fully spectrally resolved, gives a half width of  $55 \text{ m}\text{\AA}$  for the same  $\text{H}_2\text{O}$  line (which in the FTS spectrum had about the same strength as in our ZIMPOL spectra and therefore had about the same saturation effects).

The amount of smearing due to the convolution of the instrumental profile with the line profile depends critically on the shapes of these profiles. For dispersion profiles the widths add linearly, for Gaussian profiles they add quadratically. The shape

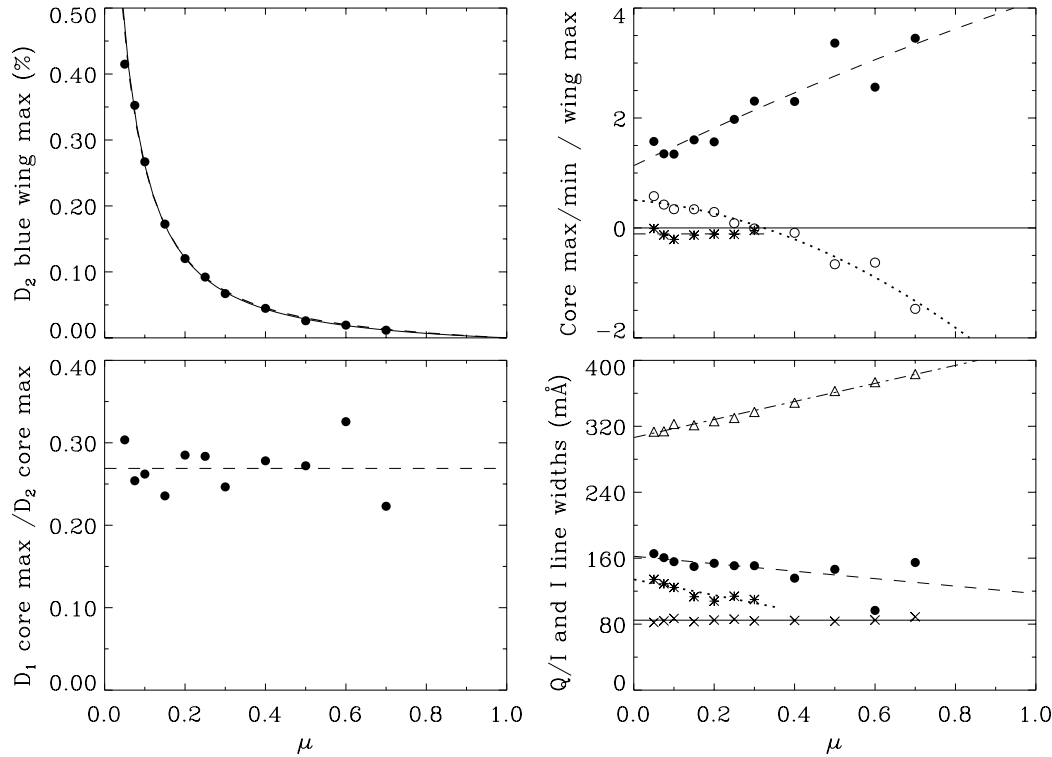


**Fig. 4.** Center-to-limb variations of the  $Q/I$  line parameters that have been extracted from the set of spectra in Fig. 1. In the panel to the upper left for the blue wing maximum in the  $D_2$  line the solid curve represents a fit to the points, while the almost identical dashed curve is 12 times the theoretical continuum polarization at this wavelength. In the panel to the upper right the filled circles represent the ratio between the polarization amplitudes in the  $D_2$  core peak and blue wing, while the open circles represent the ratio between the average value of the polarization minima surrounding the core peak and the amplitude of the blue wing. The dashed and dotted curves are second-order polynomial fits. The asterisks similarly represent the average value of the polarization minima surrounding the core peak of the  $D_1$  line, normalized to the amplitude of the  $D_2$  blue wing. The panel to the lower left gives the ratio between the polarization amplitudes in the  $D_1$  and  $D_2$  core peaks. The horizontal dashed line is the average of the points with  $\mu \leq 0.5$ . The panel to the lower right shows the total width (as defined in text) of the core polarization peak in the  $D_2$  (filled circles and dashed line) and the  $D_1$  line (asterisks and dotted line). The open triangles and dashed-dotted line represent the total width (at half the minimum level) of the  $D_1$  intensity line profile, while the crosses and the horizontal solid line give the  $\mu$ -independent line width of the  $H_2O$  telluric line at  $5891.660 \text{ \AA}$

of the telluric line is in the FTS spectrum more dispersion-like than Gaussian. With the measured total half widths of 85 and 55 mÅ in the two cases, it would follow that the half width of the instrumental profile is 30 mÅ if the profiles were dispersion-like, 65 mÅ if they were Gaussian. In practice neither of these extreme cases apply but we have something in between.

For a better quantitative estimate of the smearing function we assume that its shape is rectangular, and then vary its width as the single free parameter. A rectangular profile is chosen both for simplicity, and because the main smearing contribution comes from the projected slit width. Comparing the telluric line profile of the smoothed FTS spectrum with the same profile of our present data set, we find a good agreement when the width of the rectangular smoothing window is about 50 mÅ. This value is consistent with our previous estimate based on the slit width and considering secondary effects that may include contributions from pixel size and data reduction procedures.

From these considerations and our comparison between the smeared and unsmeared telluric line widths we estimate that

the true values for the widths of the  $D_1$  core peaks are smaller by about 25 mÅ than the values given by Eq. (5), while for the broader  $D_2$  core peak the reduction may be expected to be somewhat smaller. As we expect the peak area to be conserved, a reduced width implies a correspondingly increased peak amplitude. Since the narrower  $D_1$  peak is more affected than the  $D_2$  peak, the ratio between the  $D_1$  and  $D_2$  amplitudes that was displayed in the lower left panel of Fig. 4 is expected to increase somewhat, in favor of the  $D_1$  amplitude. This accentuates the enigma that accompanies the  $D_1$  line, which in standard quantum-mechanical scattering theory has been considered to be unpolarizable.

From the detailed profile shapes of the polarized  $D_1$  line displayed in Fig. 3 we notice that the dips forming the minima that surround the core peak are narrower than the core peak itself. We may therefore expect that the depths of these minima would increase more than the corresponding increase of the core maximum when the spectral resolution is increased. This applies to the  $D_2$  line as well.

Given the uncertainty in the shape and width of the instrumental smearing profile we will not here try to make a deconvolution of the spectra, since such deconvolutions tend to be numerically unstable (e.g. due to division by numbers that are nearly zero in the Fourier domain). Instead we recommend that when trying to model the present observational data, the theoretical profiles should first be smoothed with a rectangular window of width  $50 \text{ m}\text{\AA}$ . The so smoothed model profiles can then be used to extract the various profile parameters that may be directly compared with the empirically determined center-to-limb variations that we have presented here.

#### 4. Conclusions

Our analysis of the center-to-limb behavior of the scattering polarization in the Na I  $D_1$  and  $D_2$  lines shows that the enigmatic and narrow polarization peaks in the line cores are not a property that is restricted to the limb region, but it is a property that dominates the relative profile shape even more as we move away from the limb towards disk center. The relative core to wing amplitude ratio increases substantially with limb distance. However, the ratio between the polarization amplitudes in the  $D_1$  and  $D_2$  line cores remains approximately independent of limb distance, which is more likely to happen if these two peaks have the same physical origin.

Such a common origin is not obvious, since it is generally believed that for the Ca I 4227 and Sr II 4078  $\text{\AA}$  lines, the core polarization peaks with their surrounding minima and wing maxima are due to partial redistribution effects in the formation of these lines (Rees & Saliba 1982; Saliba 1985). Such redistribution effects are however incapable of generating the polarization seen at the core of the Na I  $D_1$  line, but a more “exotic” mechanism like that of Landi Degl’Innocenti (1998) involving optical pumping in combination with hyperfine structure splitting seems to be required. Such a mechanism however cannot work for the Ca I 4227  $\text{\AA}$  line, since its ground state is not polarizable (its quantum number  $J = 0$ ), and it has no hyperfine structure splitting (since calcium has zero nuclear spin). The appearance of the Na I  $D_2$  profile shape is rather similar to that of the Ca I 4227  $\text{\AA}$  line, but our results here support the view that the underlying physical mechanism is more closely related to the mechanism that is responsible for the  $D_1$  core peak rather than to partial redistribution physics.

As we move away from the limb, the observations of the scattering polarization become increasingly vulnerable to and affected by disturbances from the longitudinal Zeeman effect, which infiltrates the linear polarization measurements because of instrumental cross talk. Due to the ubiquitous nature of solar magnetic fields, such Zeeman-effect signals appear everywhere on the disk, but in the case of the Na I  $D_1$  and  $D_2$  lines they are much less prominent close to the limb. Still, even far from the limb, it is possible to identify these spurious spectral signatures and exclude from the analysis those portions along the slit where they occur. It is particularly remarkable to find that the pronounced core polarization peaks in the  $D_1$  and  $D_2$  lines survive practically unscathed even when they are surrounded by

magnetic flux elements everywhere, regardless of how far from the solar limb we are.

In his theory that seeks to explain the core peaks in the  $D_1$  and  $D_2$  lines Landi Degl’Innocenti (1998) concludes that the peaks can sufficiently survive magnetic depolarization effects and have as large relative amplitudes as the observed ones only if the magnetic field strengths do not exceed 0.01 G, or if the field orientation is very nearly vertical. The observations show high and apparently undisturbed core polarization peaks in environments on the solar disk, where all over the adjacent surroundings we have signals from the longitudinal Zeeman effect that are signatures of strong magnetic fields (with field strengths on the order of 1 kG, as we know from other Zeeman-effect diagnostics of photospheric flux elements, cf. Stenflo 1994). It seems highly unlikely from the point of view of plasma physics that adjacent to these kG flux tubes, side by side, we would have magnetic fields that are weaker by more than 5 orders of magnitude, or that the field lines that fill the volume between the kG flux tubes can avoid being tilted by the dynamic forces of the turbulent motions. Although the theory of magnetoturbulence is not developed well enough to have much predictive power concerning the degree of intermittency, we feel that it is physically not credible that the turbulent amplification of the magnetic field could be so suppressed that the field would not exceed 0.01 G, which is several orders of magnitude below the value that the field would have in the case of equipartition between the kinetic and magnetic energies, or that field line tilts could be prevented. An untilted or a superweak magnetic field with a large filling factor also appears to be ruled out by observations of Hanle depolarization in different spectral lines (Bianda et al. 1998a,b, 1999).

For these reasons we must conclude that we still do not have any acceptable theoretical explanation for the core polarization peaks in the Na I  $D_1$  and  $D_2$  lines. With our present work we have explored the center-to-limb variation of these polarized profiles in considerable quantitative detail. The established empirical relations may guide future theoretical efforts and provide detailed quantitative constraints on modelling attempts.

*Acknowledgements.* We wish to thank the engineering group at ETH Zurich (Peter Povel, Peter Steiner, Urs Egger, Frieder Aebersold), who built the ZIMPOL system and provided the technical support. The ZIMPOL development program and one of us (A.G.) have been funded by the Swiss Nationalfonds, grant no. 20-50464.97/1. We are also grateful to Egidio Landi Degl’Innocenti for his helpful comments on the manuscript. The National Solar Observatory, where the observations were done, is one of the National Optical Astronomy Observatories, which are operated by the Association of Universities for Research in Astronomy, Inc. (AURA) under cooperative agreement with the National Science Foundation.

#### References

- Bianda, M., Solanki, S.K., Stenflo, J.O., 1998a, A&A 331, 760
- Bianda M., Stenflo J.O., Solanki S.K., 1998b, A&A 337, 565
- Bianda M., Stenflo J.O., Solanki S.K., 1999, A&A 350, 1060
- Fluri D.M., Stenflo J.O., 1999, A&A 341, 902
- Fontenla J.M., Avrett E.H., Loeser R., 1993, ApJ 406, 319

- Giovanelli R.G., 1980, *Solar Phys.* 68, 49
- Jones H.P., Giovanelli R.G., 1983, *Solar Phys.* 87, 37
- Keller C.U., 1996, In: Stenflo J.O., Nagendra K.N. (eds.), *Solar Polarization. Proc. 1st SPW*, Kluwer, Dordrecht, p. 243 (also *Solar Phys.* 164, 243)
- Keller C.U., Sheeley N.R.Jr., 1999, In: Nagendra K.N., Stenflo J.O. (eds.), *Solar Polarization. Proc. 2nd SPW*, Kluwer, Dordrecht, p. 17 (=ASSL 243, 17)
- Landi Degl'Innocenti E., 1998, *Nature* 392, 256
- Landi Degl'Innocenti E., 1999, In: Nagendra K.N., Stenflo J.O. (eds.), *Solar Polarization. Proc. 2nd SPW*, Kluwer, Dordrecht, p. 61 (=ASSL 243, 61)
- Omont A., Smith E.W., Cooper J., 1973, *ApJ* 182, 283
- Povel H.P., 1995, *Optical Engineering* 34, 1870
- Rees D.E., Saliba G.J., 1982, *A&A* 115, 1
- Saliba G.J., 1985, *Solar Phys.* 98, 1
- Stenflo J.O., 1980, *A&A* 84, 68
- Stenflo J.O., 1994, *Solar Magnetic Fields – Polarized Radiation Diagnostics*. Kluwer, Dordrecht
- Stenflo J.O., 1997, *A&A* 324, 344
- Stenflo J.O., 1998, *A&A* 338, 301
- Stenflo J.O., Keller C.U., 1996, *Nature* 382, 588
- Stenflo J.O., Keller C.U., 1997, *A&A* 321, 927
- Stenflo J.O., Baur T.G., Elmore D.F., 1980, *A&A* 84, 60
- Stenflo J.O., Twerenbold D., Harvey J.W., et al., 1983, *A&AS* 54, 505
- Stenflo J.O., Keller C.U., Gandorfer A., 1998, *A&A* 329, 319